–0.95 (m, CH_2CH_2CH), –2.46 (CHOH), –2.5 (s, 2 × NH).

Iron(III) Derivatives (11–14). Iron complexes were synthesized in dimethylformamide by using anhydrous iron(II) chloride and purified as previously described.[21b] Chloroiron(III) and hydroxyiron(III) derivatives were generated by shaking a toluene solution of the metalloporphyrins with aqueous sodium chloride and aqueous sodium carbonate, respectively.

Acknowledgment. This work was supported by the Institut National de la Santé et de la Recherche Médicale.

Contribution from the Department of Chemistry and the Molecular Structure Center, Indiana University, Bloomington, Indiana 47405, and the Department of Chemistry, Manchester University, Manchester M13 9PL, U.K.

Isolation and Structure of $[V(OSiMe_3)(edt)_2]^-$ (edt^{2-} = Ethane-1,2-dithiolate), an Intermediate in the Conversion of $[VO(edt)_2]^{2-}$ to $[VS(edt)_2]^{2-}$ with $(Me_3Si)_2S$. EPR Characterization of the Series $[VE(LL)_2]^{z-}$ (E = O, S, $OSiMe_3$, LL = edt; E = O, LL = pdt)

Joanna K. Money,[1a] Kirsten Folting,[1b] John C. Huffman,[1b] David Collison,[1c] John Temperley,[1c] Frank E. Mabbs,*[1c] and George Christou*[1a]

Received June 12, 1986

The isolation and crystal structure of an intermediate in the conversion of $[VO(edt)_2]^{2-}$ (edt = ethane-1,2-dithiolate) to $[VS(edt)_2]^{2-}$ with $(Me_3Si)_2S$ is reported. $(PPh_4)[V(OSiMe_3)(edt)_2]$ crystallizes in triclinic space group $P\bar{1}$ with a = 12.694 (4) Å, b = 14.901 (5) Å, c = 8.944 (2) Å, α = 96.87 (2)°, β = 94.15 (2)°, γ = 104.30 (2)°, and Z = 2. The anion contains a discrete, five-coordinate, approximately square-pyramidal vanadium(IV) center with V–O = 1.7608 (27) Å, mean V–S = 2.322 Å and mean O–V–S = 107.39°. Fluid and frozen solution EPR spectra on the series $[VE(edt)_2]^{2-}$ (E = O, S, $OSiMe_3$) and on $[VO(pdt)_2]^{2-}$ (pdt = propane-1,3-dithiolate) at X-band frequencies are reported. These data in conjunction with the electronic absorption spectra have been interpreted in terms of a molecular orbital scheme for the antibonding metal d orbitals in the complexes.

Introduction

Recently we reported the preparation, structures and some properties of the vanadium thiolate anions $[VE(edt)_2]^{2-}$ (edt^{2-} = ethane-1,2-dithiolate; E = O (**1**), E = S (**2**)).[2] These species are five-coordinate and square pyramidal with the multiply bonded atom occupying the apical position and four thiolate sulfur atoms occupying the basal positions. Our interest in such species is threefold: (i) to redress the lack of characterized thiolate complexes in the otherwise well-explored area of vanadium(IV) chemistry; (ii) to have at hand vanadium–thiolate species that could act as models for any vanadium–cysteine linkages which might be detected in biological systems; (iii) to investigate the possibility of using mononuclear vanadium thiolates as "building-blocks" for the assembly of higher nuclearity vanadium aggregates. In the latter respect the synthesis of **2** was particularly desirable over **1** in that it contains the highly reactive thiovanadyl (VS^{2+}) unit, allowing the possibility of generating unknown $[V/S/SR]_n$ ($n \geq 2$) species.

Complex **1** was converted to **2** by treatment with hexamethyldisilathiane, $(Me_3Si)_2S$. We herein report the trapping, isolation, and structural characterization of an intermediate in this conversion, $[V(OSiMe_3)(edt)_2]^-$ (**3**). This species provides further progress toward objective i and represents another highly reactive potential "building-block" toward objective iii. In addition, the identification of **3** provides an illuminating insight into the mechanistic pathway from **1** to **2**. We also report the detailed characterization by electron paramagnetic resonance (EPR) spectroscopy of the three-membered series $[VE(edt)_2]^z$ (E = O, S, $OSiMe_3$), a rare opportunity to investigate the effects of varying apical groups in three complexes possessing a basal ligand constancy, and of the related compound $[VO(pdt)_2]^{2-}$ (pdt^{2-} is propane-1,3-dithiolate).

Experimental Section

All manipulations were performed with use of standard inert-atmosphere techniques and a purified dinitrogen atmosphere. Acetonitrile (CaH_2) and diethylether (Na/benzophenone) were distilled and degassed prior to use. $NaSSiMe_3$ was prepared as described elsewhere.[3] Hexamethyldisilathiane (Petrarch) was used as received. $(PPh_4)Na[VO(edt)_2]\cdot 2EtOH$ and $(PPh_4)Na[VS(edt)_2]\cdot xEt_2O$ were available from previous work.[2]

Synthesis of $(PPh_4)[V(OSiMe_3)(edt)_2]$. A slurry of green $(PPh_4)Na[VO(edt)_2]\cdot 2EtOH$ (703 mg, 1 mmol) in MeCN (15 mL) was treated with excess hexamethyldisilathiane (2.0 mL, 9.5 mmol). The green solid rapidly dissolved, and an intense red-purple homogeneous solution was obtained. A large excess of ether (225 mL) was then added as quickly as possible to begin precipitation of a black solid, and the mixture was cooled to –20 °C in a freezer for 1 h. The crude product, contaminated with traces of the thiovanadyl species (**2**), was collected by filtration, washed with ether, and dried in vacuo. The solid was dissolved in room-temperature MeCN (25 mL) and filtered, and ether (175 mL) was added. Overnight storage at –20 °C yielded the analytically pure material as well-formed black prisms in 28% overall yield. Anal. Calcd for $C_{31}H_{37}OPS_4SiV$: C, 56.09; H, 5.62; S, 19.32. Found: C, 56.23; H, 5.81; S, 19.59.

Conversion of $[V(OSiMe_3)(edt)_2]^-$ to $[VS(edt)_2]^{2-}$ with $NaSSiMe_3$. A solution of $(PPh_4)[V(OSiMe_3)(edt)_2]$ (0.081 g, 0.12 mmol) in MeCN (10 mL) was treated with 1 equiv of $NaSSiMe_3$ (0.016 g, 0.12 mmol). The red-purple color slowly changed to orange-brown. After a total of 36 h, ether (15 mL) was added to precipitate a fine brown solid. This was collected by filtration, washed with ether, and dried. Its infrared spectrum was identical with that of authentic $(PPh_4)Na[VS(edt)_2]\cdot xEt_2O$.

Synthesis of $Na_4(acac)_2[VO(pdt)_2]\cdot 2DMF$. A solution of Na_2pdt (45 mmol) in EtOH (100 mL) was prepared from the dithiol (4.52 mL, 45 mmol) and Na metal (2.07 g, 90 mmol). Solid $VO(acac)_2$ (2.98 g, 11.3 mmol) was added with stirring, and as it dissolved a green solution was formed, which rapidly precipitated a light green solid. The solid was collected by filtration, washed with EtOH, and dried in vacuo. Recrystallization from DMF/Et_2O produced long green needles of analytically pure product in 40% overall yield. The presence of monomeric $[VO(pdt)_2]^{2-}$ in this complex salt was confirmed by a crystal structure determination (unpublished work). Anal. Calcd for

(1) (a) Department of Chemistry, Indiana University. (b) Molecular Structure Center, Indiana University. (c) Manchester University.
(2) Money, J. K.; Huffman, J. C.; Christou, G. *Inorg. Chem.* **1984**, *24*, 3297.
(3) Do, Y.; Simhon, E. D.; Holm, R. H. *Inorg. Chem.* **1983**, *22*, 3809.

0020-1669/86/1325-4583$01.50/0

Table I. Crystallographic Data for $(PPh_4)[V(OSiMe_3)(edt)_2]$

formula	$C_{31}H_{37}OPS_4SiV$
M_r	663.41
cryst system	triclinic
space group	$P\bar{1}$
temp, °C	−161
a, Å	12.694 (4)[a]
b, Å	14.901 (5)
c, Å	8.944 (2)
α,deg	96.87 (2)
β, deg	94.15 (2)
γ, deg	104.30 (2)
Z	2
V, Å^3	1618.35
radiation	Mo Kα (0.71069 Å)
abs coeff, cm^{-1}	6.523
crystal size, mm	0.20 × 0.20 × 0.20
scan speed, deg min^{-1}	4.0
scan width, deg	1.8 + dispersion
scan range, deg	$6 \le 2\theta \le 45$
no. of unique intens	4248
no. of obsd. intens ($F > 3\sigma(F)$)	3496
R, %	4.06
R_w, %	4.17
goodness of fit	0.90

[a] Thirty reflections at −161 °C.

$C_{22}H_{40}N_2O_7S_4Na_4V$: C, 36.92; H, 5.63; N, 3.91; S, 17.92; V, 7.12. Found: C, 37.24; H, 6.30; N, 3.83; S, 17.78; V, 6.86. IR (nujol mull): ν(V=O) 919 cm^{-1}.

Synthesis of $(NMe_4)Na[VO(pdt)_2]\cdot 2MeOH$. Solid $VOSO_4\cdot 1.3H_2O$ (2.10 g, 11.3 mmol) was added to Na_2pdt (45 mmol), prepared as described above, in MeOH (100 mL). The slurry was stirred for 2 h, and when all the $VOSO_4$ had dissolved, NMe_4Cl (2.47 g, 22.5 mmol) was added. Addition of Et_2O (100 mL) and storage overnight at −20 °C gave green flakes, which were collected by filtration and recrystallized from $MeOH/Et_2O$ to yield the product in 30% overall yield. IR (Nujol null): ν(V=O) 929 cm^{-1}. The PPh_4^+ salt has been prepared similarly by using PPh_4Br (9.45 g, 22.5 mmol) and was obtained as the bis EtOH solvate after recrystallization from hot EtOH. Anal. Calcd for $C_{34}H_{44}O_3PS_4NaV$: C, 55.65; H, 6.04. Found: C, 54.77; H, 5.73.

X-ray Crystallography and Structure Solution. Data were collected at approximately −161 °C; details of the diffractometry, low-temperature facilities, and computational procedures employed by the Molecular Structure Center are available elsewhere.[4] Data collection parameters are summarized in Table I. A systematic search of a limited hemisphere of reciprocal space yielded a set of reflections that exhibited no symmetry and no systematic extinctions. The triclinic space group $P\bar{1}$ was chosen and confirmed by the subsequent solution and refinement of the structure.

The structure was solved by a combination of direct methods (MULTAN) and Fourier techniques, and refined by full-matrix least squares. The compound crystallizes in triclinic space group $P\bar{1}$, with the asymmetric unit containing the complete anion and cation pair. Non-hydrogen atoms were readily located and refined with anisotropic thermal parameters. In the latter stages all hydrogen atoms were located in a difference Fourier synthesis. They were included in the final refinement cycles with isotropic thermal parameters. The final difference Fourier map was essentially featureless, the largest peak being 0.4 e/Å^3. Final values of discrepancy indices R and R_w are included in Table I.

Electron Paramagnetic Resonance (EPR) Spectra. Spectra were obtained on fluid and frozen solutions of the compounds in appropriate dried deoxygenated solvents at room temperature and 77 K at X-band frequencies with a Varian E112 spectrometer. Low temperatures were obtained by using an Oxford Instruments ESR9 continuous-flow cryostat with liquid nitrogen as coolant. The results are listed in Tables V and VI.

Other Measurements. Infrared spectra were recorded as Nujol mulls on a Perkin-Elmer Model 283 spectrophotometer. Electronic spectra were obtained in DMF solution on a Perkin-Elmer Model 330 spectrophotometer.

Results and Discussion

Synthesis. In our earlier report[2] we described the clean conversion of green $[VO(edt)_2]^{2-}$ (**1**) to orange-brown $[VS(edt)_2]^{2-}$

(4) Chisholm, M. H.; Folting, K.; Huffman, J. C.; Kirkpatrick, C. C. *Inorg. Chem.* **1984**, *23*, 1021.

Table II. Fractional Coordinates[a] and Isotropic Thermal Parameters

atom	x	y	z	B[b]
V(1)	7686 (1)	2236.0 (5)	3947 (1)	11
S(2)	7841 (1)	1634 (1)	1463 (1)	14
C(3)	8794 (4)	2678 (3)	1002 (5)	19
C(4)	9826 (4)	2898 (3)	2066 (5)	21
S(5)	9517 (1)	2988 (1)	4034 (1)	16
S(6)	6567 (1)	759 (1)	4037 (1)	15
C(7)	6566 (4)	644 (3)	6061 (5)	20
C(8)	6839 (4)	1581 (3)	7029 (5)	21
S(9)	8107 (1)	2326 (1)	6543 (1)	19
O(10)	6888 (2)	3039 (2)	3780 (3)	15
Si(11)	6806 (1)	4082 (1)	4557 (1)	16
C(12)[c]	5919 (4)	3935 (3)	6113 (5)	27
C(13)[c]	8180 (4)	4826 (3)	5348 (6)	23
C(14)[c]	6195 (4)	4605 (3)	3039 (6)	30
P(15)	7773 (1)	−2021 (1)	2242 (1)	11
C(16)[d]	6710 (3)	−1756 (3)	1081 (4)	13
C(17)	5646 (3)	−2357 (3)	868 (5)	16
C(18)	4827 (3)	−2120 (3)	10 (5)	18
C(19)	5056 (3)	−1292 (3)	−619 (5)	17
C(20)	6086 (3)	−698 (3)	−385 (5)	16
C(21)	6926 (3)	−925 (3)	455 (4)	14
C(22)[d]	8987 (3)	−1072 (3)	2391 (4)	13
C(23)	9835 (3)	−1156 (3)	1538 (5)	18
C(24)	10745 (4)	−397 (3)	1597 (5)	23
C(25)	10781 (4)	432 (3)	2487 (5)	23
C(24)	10745 (4)	−397 (3)	1597 (5)	23
C(25)	10781 (4)	432 (3)	2487 (5)	23
C(26)	9926 (4)	525 (3)	3319 (5)	19
C(27)	9032 (3)	−229 (3)	3282 (5)	15
C(28)[d]	8083 (3)	−3086 (3)	1435 (4)	13
C(29)	7431 (3)	−3672 (3)	208 (5)	16
C(30)	7687 (4)	−4492 (3)	−354 (5)	20
C(31)	8575 (4)	−4733 (3)	303 (5)	22
C(32)	9223 (4)	−4153 (3)	1519 (5)	21
C(33)	8992 (3)	−3326 (3)	2096 (5)	15
C(34)[d]	7273 (3)	−2164 (3)	4061 (4)	12
C(35)	6489 (3)	−1710 (3)	4535 (5)	15
C(36)	6072 (3)	−1833 (3)	5897 (5)	15
C(37)	6436 (3)	−2411 (3)	6799 (4)	15
C(38)	7216 (4)	−2859 (3)	6348 (5)	17
C(39)	7634 (3)	−2741 (3)	4982 (5)	16

[a] ×10^4. [b] Å^2 × 10. [c] Silicon-bound methyl carbons. [d] Carbon atoms C(16), C(22), C(28), and C(34) are bound to the phosphorus. Other phenyl carbons are numbered consecutively around the ring.

Table III. Selected Bond Lengths (Å) and Angles (deg) for **3**

	(a) Bonds		
V–S(2)	2.3352 (14)	S(2)···S(5)	3.154 (2)
V–S(5)	2.3094 (15)	S(6)···S(9)	3.187 (2)
V–S(6)	2.3199 (15)	S(2)···S(6)	3.136 (2)
V–S(9)	2.3248 (14)	S(5)···S(9)	3.138 (2)
mean	2.322 (9)	mean	3.154 (20)
V–O(10)	1.7608 (27)	Si(11)–O(10)	1.655 (3)
	(b) Angles		
O(10)–V–S(2)	105.27 (10)	S(2)–V–S(5)	85.53 (5)
O(10)–V–S(5)	110.00 (10)	S(2)–V–S(6)	84.69 (5)
O(10)–V–S(6)	110.06 (10)	S(5)–V–S(9)	83.13 (5)
O(10)–V–S(9)	104.23 (10)	S(6)–V–S(9)	86.64 (5)
mean	107.39 (2.67)	mean	85.00 (1.28)
S(2)–V–S(9)	150.47 (5)	V–O(10)–Si(11)	140.82 (18)
S(5)–V–S(6)	139.93 (5)		

Table IV. Comparison of Selected Structural Parameters of **1**–**3**

	1	**3**	**2**
V–E,[a] Å	1.625 (2)	1.7608 (27)	2.087 (1)
V–S,[b] Å	2.378	2.322	2.364
S–V–S,[b] deg	85.56	85.00	83.76
S–V–E,[b] deg	106.34	107.39	109.41
V–S_4,[c] Å	0.668	0.693	0.784

[a] E = O (**1**), $OSiMe_3$ (**3**), or S (**2**). [b] Mean of four values. [c] Vanadium to S_4 least-squares plane.

Table V. X-Band Fluid-Solution Data[a] (at 298 K)

compound	solvent	g_{iso}	-10^4A_{iso}, cm^{-1}
$(Me_4N)Na[VO(edt)_2]$	DMF	1.981	71.6
	Me_2SO	1.980	72.2
	CH_3CN	1.981	72.4
	CH_3OH	1.981	76.6
$(Ph_4P)Na[VS(edt)_2]$	DMF	1.972	64.6
	Me_2SO	1.973	64.5
	CH_3CN	1.972	64.3
$(Ph_4P)[V(OSiMe_3)(edt)_2]$	DMF	1.976	53.5
	Me_2SO	1.976	53.5
	CH_3CN	1.977	53.7
$Na_4(acac)_2[VO(pdt)_2]$	DMF	1.977	72.9
	Me_2SO	1.977	75.0
$(Me_4N)Na[VO(pdt)_2]$	Me_2SO	1.978	74.6
	CH_3CN	1.979	74.8
	CH_3OH	1.981	70.7

[a] Estimated errors on g values ±0.002 and on A values of ±0.5 × 10^{-4} cm^{-1}.

(**2**) by using $(Me_3Si)_2S$, as summarized in eq 1. It was mentioned

$$[VO(edt)_2]^{2-} + (Me_3Si)_2S \rightarrow [VS(edt)_2]^{2-} + (Me_3Si)_2O \quad (1)$$

that intermediate to the formation of **2** was the immediate appearance of an intense red-purple coloration, which slowly converted to orange-brown on continued reaction. We have since noticed that the presence of excess $(Me_3Si)_2S$ slows the latter reaction somewhat. For reasons already outlined in the Introduction, and to gain mechanistic insight into the conversion of **1** to **2**, we decided to seek the isolation and identification of the red-purple intermediate. Reaction of **1** with 9.5 equiv of $(Me_3Si)_2S$, addition of an excess of ether as quickly as was practically possible, and cooling to −20 °C yielded the intermediate as a black precipitate contaminated with some complex **2**. Recrystallization from $MeCN/Et_2O$ yielded analytically pure product as black prisms. An X-ray crystallographic study showed this to be the vanadium(IV) monomer $(PPh_4)[V(OSiMe_3)(edt)_2]$, (PPh_4)(**3**).

Description of Structure. Fractional atomic coordinates for the non-hydrogen atoms are listed in Table II. Selected bond lengths and angles are listed in Table III. An ORTEP projection of **3** is depicted in Figure 1; the structure of the PPh_4^+ cation is unexceptional and will not be discussed further. The anion **3** contains a five-coordinate vanadium(IV) in square-pyramidal geometry. Four dithiolate sulfur atoms occupy basal positions with the metal 0.693 Å above the least-squares plane (maximum deviation by S(5), 0.101 Å). The apical position is occupied by oxygen atom O(11) of the Me_3SiO^- group. O–V–S and S–V–S angles are in the fairly narrow range 104.23–110.06 and 83.13–86.64°, respectively, emphasizing the close approach of the VOS_4 core to C_{4v} symmetry. The structures of **1**–**3** are thus the same except for the apical ligands; corresponding structural data for the three anions are compared in Table IV. Of immediate interest is the axial V–$OSiMe_3$ distance, 1.7608 (27) Å, which is significantly lengthened relative to that in **1**. This is consistent with conversion of multiply bonded V=O to essentially singly bonded V—$OSiMe_3$ with major loss of oxygen-to-vanadium π-donation. Similar bond lengths for V–$OSiMe_3$ are observed in $V(NR)(OSiMe_3)_3$ (1.762 (2)–1.766 (2) Å; R = 1-adamantyl).[5] On conversion to **2** the resulting V=S bond is even longer, as expected from the greater size of S vs. O. The loss of axial π-electron donation in **3** also results in a shortening of basal V–S bonds compared to those in **1** and **2**. This could be due to a compensatory increase in sulfur-to-metal π-donation or simply to the increase in the net positive charge at the vanadium, or both. In contrast, inspection of Table IV shows that almost insignificant angular changes accompany trimethylsilation of the oxygen atom of **1** with larger but still small changes on conversion to **2**. The V–O–Si angle of 140.82 (18)° is somewhat smaller than those in $V(NR)(OSiMe_3)_3$ (148.7 (1)–154.1 (1)°),[5] but is otherwise typical of silicon-bound oxygen. Si–O–Si angles in the disilylethers $R_3Si–O–SiR_3$ are in the range 140–180° attributed to overlap between filled oxygen p_π orbitals and empty silicon d orbitals. The exact angle that may be observed is also dependent on steric factors if the R groups are bulky.[6]

Anion **3** represents a very rare example of true five-coordination in vanadium(IV) chemistry, i.e. five formally single bonds. Although complexes of formulation VL_5 are not uncommon for this oxidation state, structural characterization usually shows that dimeric $L_4V(\mu\text{-}L)_2VL_4$ units are present with six-coordination at the metal.[6] $[VCl_5]^-$ is another example of true five-coordination,[7] and in this case the geometry is trigonal bipyramidal with axial Cl–V–Cl equal to 179.4°.

EPR and Electronic Absorption Spectra. The spin-Hamiltonian parameters in Tables V and VI were obtained by spectrum simulation based on methods outlined previously.[8,9] Two examples of the comparison between observed and simulated spectra are given in Figures 2 and 3. Because of limitations on the solubility and on the quality of the frozen-glass spectra it has not been possible to obtain measurements on all of the compounds in one single solvent system. The A_{iso} values for the oxovanadium(IV) complexes show some solvent dependence, which suggests solvent molecule binding. However, where we have been able to obtain sufficiently high quality data, this solvent variation does not seem to persist in frozen solution for $[VO(edt)_2]^{2-}$. We also attempted to obtain frozen-solution spectra at Q-band frequencies. However, because of the oxygen sensitivity of the compounds, we only obtained satisfactory spectra for $(Me_4N)Na[VO(edt)_2]$. The spectrum at the higher frequency was almost identical with that at X-band, thus confirming the essentially isotropic **g** tensor; see Figure 2.

The spin-Hamiltonian parameters in Table VI were obtained from the spectrum simulations, assuming coincident **g** and **A** tensor axes. The crystallographic data on all of the compounds do not *require* the anions to have symmetry higher than C_s, although geometrically deviations from C_{4v} point symmetry are not large. In C_s point symmetry there is no requirement for coincidence between the **g** and **A** tensor axes. However, we found that we could not improve the spectrum simulations by allowing noncoincidence of the axes of these two tensors. Thus, throughout the remainder of the discussion we will assume coincident **g** and **A** tensor axes and for continuity of the treatment we also assume effective C_{2v} point symmetry for all of the anions despite some of them having an axially symmetric **A** tensor.

The changes in the spin-Hamiltonian parameters and in the electronic absorption spectra on going from $[VO(edt)_2]^{2-}$ to $[VS(edt)_2]^{2-}$ are qualitatively similar to those observed in the series [VEL], where E = O, S and L = salen, acen.[10] Similarly, reduction in the magnitudes of the hyperfine parameters on going from $[VO(edt)_2]^{2-}$ to $[V(OSiMe_3)(edt)_2]^-$ is qualitatively similar to the changes found in replacing VO by *trans*-VCl_2 in some $[VOL_4]$ and $[VCl_2L_4]$ compounds,[11] where L_4 = a tetradentate ligand or two bidentate ligands.

The electronic spectra of complexes **1**–**3** were obtained in DMF solution. The band maxima, their extinction coefficients, and their proposed assignments are collected in Table VII. The assignments are based on the interpretation of changes in band maxima as the terminal group is changed and partly on the apparent extinction coefficients, and are also made by comparison with the spectra of other known five-coordinate square-pyramidal oxovanadium(IV) compounds. Mull and single-crystal polarized electronic absorption spectra in the temperature range 4.2–300 K on a number of well-characterized square-pyramidal oxovanadium(IV) compounds[12] have established that all the d–d bands in such systems are likely to occur below ca. (25–30) × 10^3 cm^{-1}. Conversion of

(5) Nugent, W. A.; Harlow, R. L. *J. Chem. Soc., Chem. Commun.* **1979**, 342.
(6) Cotton, F. A.; Wilkinson, G. *Advanced Inorganic Chemistry*, Wiley-Interscience: New York, 1980.
(7) Ziegler, M. L.; Nuber, B.; Weidenhammer, K.; Hoch, G. *Z. Naturforsch., B: Anorg. Chem. Org. Chem.* **1977**, *32B*, 18.
(8) Collison, D.; Mabbs, F. E. *J. Chem. Soc., Dalton Trans.* **1982**, 1525.
(9) Gahan, B.; Mabbs, F. E. *J. Chem. Soc., Dalton Trans.* **1983**, 1713.
(10) Callahan, K. P.; Durand, P. J. *Inorg. Chem.* **1980**, *19*, 3211.
(11) Jezierski, A.; Raynor, J. B. *J. Chem. Soc., Dalton Trans.* **1981**, 3211.

Table VI. X-Band Frozen-Solution Data (at 77 K)

compounds	solvent(s)	g_{xx}[a]	g_{yy}[a]	g_{zz}[a]	-10^4A_{xx},[b] cm^{-1}	-10^4A_{yy},[b] cm^{-1}	-10^4A_{zz},[b] cm^{-1}	$\langle g\rangle$[c]	$-10^4\langle A\rangle$,[d] cm^{-1}
$(Me_4N)Na[VO(edt)_2]$[e]	Me_2SO, DMF, CH_3OH	1.978	1.977	1.976	39.7	39.7	133.8	1.977	71.1
$(Ph_4P)Na[VS(edt)_2]$	DMF	1.966	1.971	1.978	36.7	35.3	122.4	1.972	64.8
	Me_2SO	1.971	1.960	1.976	35.3	35.1	120.6	1.969	63.7
$(Me_4N)Na[VO(pdt)_2]$	CH_3OH	1.978	1.977	1.976	39.7	39.7	132.8	1.977	70.7
$Na_4(acac)_2[VO(pdt)_2]$	DMF, Me_2SO	1.976	1.978	1.970	40.6[f]	39.7	137.2	1.975	72.5
$(Ph_4P)[V(OSiMe_3)(edt)_2]$	CH_3CN, DMF	1.967	1.962	1.990	26.4[g]	13.8	113.2	1.973	51.1

[a] Estimated errors on g values ±0.002. [b] Estimated errors on A values $\pm0.5 \times 10^{-4}$ cm^{-1}. [c] $\langle g\rangle = {}^1/_3(g_{xx} + g_{yy} + g_{zz})$. [d] $\langle A\rangle = {}^1/_3(A_{xx} + A_{yy} + A_{zz})$. [e] Parameters also simulate the frozen-solution spectrum at Q-band in Me_2SO at 150 K. [f] Estimated error $\pm1.0 \times 10^{-4}$ cm^{-1}. [g] Estimated error $\pm3.0 \times 10^{-4}$ cm^{-1}.

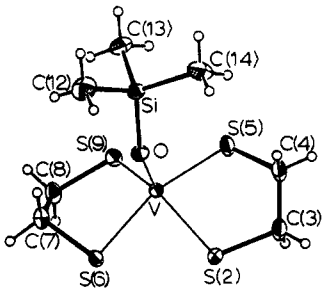

Figure 1. ORTEP projection of complex **3** showing the heavy-atom-labeling scheme. Non-hydrogen atoms are depicted as 50% probability ellipsoids; hydrogen atoms are depicted as spheres of arbitrary size.

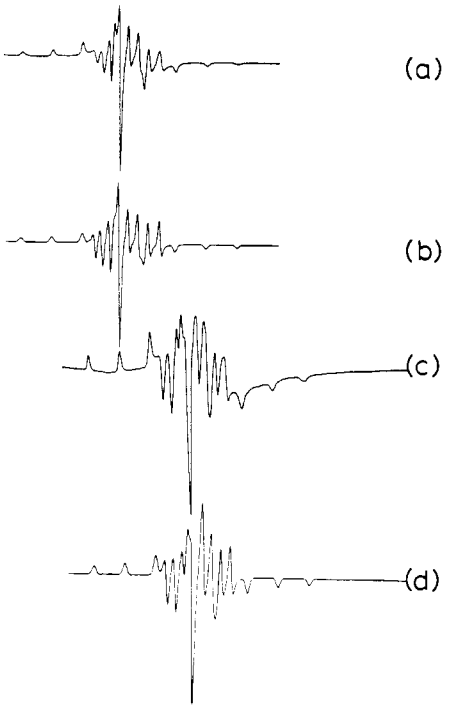

Figure 2. Frozen-solution EPR spectra of complex **1** in Me_2SO: (a) X-band experimental at 77 K; (b) X-band simulated with spin-Hamiltonian parameters from Table VI; (c) Q-band experimental at 150 K; (d) Q-band simulated with spin-Hamiltonian parameters from Table VI.

1 to **2** shifts all bands to lower energy.[2] This effect has been seen previously in, for example, VE(acen) (E = O, S),[10] and was indeed predicted, before any VS^{2+} species had been synthesized, from theoretical calculations on hypothetical $VECl_4^{2-}$ (E = O, S, Se).[13] Interpretation of the spectrum of **3** is less clear-cut. The lowest energy band is assigned to the $d_{x^2-y^2} \rightarrow d_{xz}, d_{yz}$ transition (axes defined in Figure 4) and is consistent with the observation that

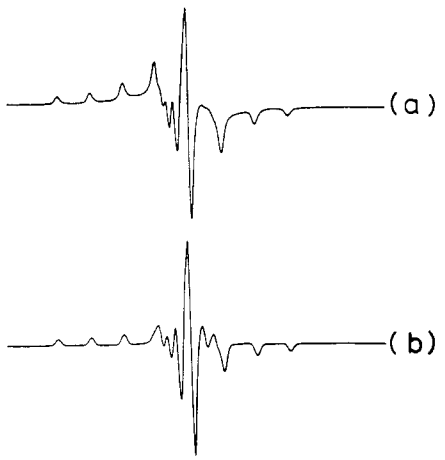

Figure 3. Frozen-solution EPR spectra of complex **3** in MeCN,X-band: (a) experimental at 77 K; (b) simulated with spin-Hamiltonian parameters from Table VI.

it decreases in energy on going from VO to VS to $VOSiMe_3$. This ordering parallels the π-donor ability to the axial group, which would be expected to decrease the energy separation between the ground state and the d_{xz}, d_{yz} orbitals. The next two bands maxima are also assigned as d–d bands although their intensities are somewhat large, and it is possible that they are due to lower energy charge-transfer transitions with the weaker d–d bands obscured. Unfortunately, similar five-coordinate vanadium(IV) sulfur complexes are not available for comparison at the present time.

The spin-Hamiltonian parameters have been interpreted via an empirical molecular orbital description of the antibonding d orbitals in the compounds (see the Appendix for the relevant equations). This treatment assumes only contributions to the **g** and **A** tensor elements that arise from the ground state and essentially metal d-orbital-based excited states. The possible involvement of ligand-to-metal charge-transfer excited states, which may give contributions of opposite sign, has not been included.[14,15]

The observed hyperfine parameters have been analyzed to give the composition of the ground state via the NAG algorithm EO4UAF,[16] which is designed to minimize a function with continuous first and second derivatives. The variables are subjected to fixed bounds with provision for equality, inequality, and range constraints. Solutions to eq A1 are required so that values of α_1, α_1', c_1, c_2, c_s, P, and κ form a consistent set, from which the observed A values can be calculated, *via* eq A14–A17, to within the limits of experimental error. The values of P were constrained to be within the range $100 \le P \times 10^4$ cm$^{-1} \le 180$.[17] The minimization was subjected to (a) the equalities in equation A2, (b) $0 \le \alpha_1 \le 1.0$, and (c) the ranges $|A_{calcd} - A_{obsd}| \le \rho$, where ρ is an acceptable tolerance between A_{calcd} and A_{obsd}, for eq A14–A17. The function

(12) Collison, D.; Gahan, B.; Garner, C. D.; Mabbs, F. E. *J. Chem. Soc., Dalton Trans.* **1980**, 667.
(13) Wasson, J. R.; Hall, J. W.; Hatfield, W. E. *Transition Met. Chem. (Weinheim, Ger.)* **1978**, *3*, 195.
(14) Glarus, S. H. *J. Chem. Phys.* **1963**, *39*, 3141.
(15) Garner, C. D.; Mabbs, F. E. *J. Inorg. Nucl. Chem.* **1979**, *41*, 1125. Garner, C. D.; Hillier, I. H.; Mabbs, F. E.; Taylor, C.; Guest, M. F. *J. Chem. Soc., Dalton Trans.* **1976**, 2258.
(16) NAG Library, Regional Computer Centre, University of Manchester, U.K.
(17) McGarvey, B. R. *J. Phys. Chem.* **1967**, *71*, 51.

Table VII. Electronic Absorption Spectra in DMF

peak maxima, cm^{-1}	extinction coeff, $dm^3\ mol^{-1}\ cm^{-1}$	proposed assignt
	$[VO(edt)_2]^{2-}$ (1)	
16 080	75	$d_{x^2-y^2} \rightarrow d_{xz}, d_{yz}$
18 180 sh	~50	$d_{x^2-y^2} \rightarrow d_{xy}$
25 000	500	$d_{x^2-y^2} \rightarrow d_{z^2}$
32 050	3600	charge transfer
	$[VS(edt)_2]^{2-}$ (2)	
11 100	80	$d_{x^2-y^2} \rightarrow d_{xz}, d_{yz}$
13 890 sh	~115	$d_{x^2-y^2} \rightarrow d_{xy}$
19 050 sh	~1000	$d_{x^2-y^2} \rightarrow d_{z^2}$
23 900	5000	charge transfer
	$[V(OSiMe_3)(edt)_2]^-$ (3)	
10 526	142	$d_{x^2-y^2} \rightarrow d_{xz}, d_{yz}$
18 620	2870	$d_{x^2-y^2} \rightarrow d_{xy}$
21 052 sh	~2375	$d_{x^2-y^2} \rightarrow d_{z^2}$
28 170	5172	charge transfer

Table VIII. Ground-State Molecular Orbital Parameters[a]

solvent(s)	α_1	α_1'	c_1	c_2	c_s	10^4P, cm^{-1}
		$(Me_4N)Na[VO(edt)_2]$				
Me_2SO, DMF, MeOH	1.000	0.066	1.000	0.000	0.000	105.8
		$(Ph_4P)Na[VS(edt)_2]$				
(i) DMF	1.000	0.053	0.996	0.004	0.055	100.0
(ii) Me_2SO	0.977	0.211	0.999	0.008	0.066	104.9
		$(Me_4N)Na[VO(pdt)_2]$				
MeOH	1.000	0.043	1.000	0.000	0.000	106.5
		$Na_4(acac)_2[VO(pdt)_2]$				
Me_2SO, DMF	0.971	0.283	1.000	0.003	0.058	116.8
		$(Ph_4P)[V(OSiMe_3)(edt)_2]$				
MeCN, DMF	0.950	0.312	0.998	0.063	0.136	121.4

[a] Fixed values of $\kappa = 0.66$ and $A_{4s} = 0.15\ cm^{-1}$ were used in these calculations. The parameters in the table were derived with ρA equal to the estimated experimental errors.

that was minimized was a weighted composite function, F, of the hyperfine parameters

$$F = \frac{(F')^{1/2}}{n}$$

where $n = 4$ (the number of hyperfine values used, eq A14–A17) and

$$F' = \left(\frac{\delta A_{zz}}{\rho A_{zz}}\right)^2 + \left(\frac{\delta A_{xx}}{\rho A_{xx}}\right)^2 + \left(\frac{\delta A_{yy}}{\rho A_{yy}}\right)^2 + \left(\frac{\delta \bar{A}}{\rho \bar{A}}\right)^2$$

where $\delta A = A_{calcd} - A_{obsd}$ and ρA is the user acceptable tolerance between each A_{calcd} and A_{obsd}.

The results of these calculations are given in Table VIII. In the analysis we have used a value of $\kappa = 0.66$ for each of the compounds. This value was obtained from the hyperfine parameters of the frozen-solution spectrum of **1** by assuming effective C_{4v} symmetry for the complex. This assumption is a reasonable approximation based on the observed axial symmetry of the A tensor. The assumption of C_{4v} symmetry resticts c_2 and c_s to be zero for this particular ion. Our value of κ is lower than that estimated for a number of other axial systems with non-sulfur-containing ligands.[11,18,20] For the anions that do not have an axially symmetric A tensor we have used a fixed value of $A_{4s} = 0.15\ cm^{-1}$.[21] As we may have anticipated from the similarity of the spin-Hamiltonian parameters there is little difference in the composition of the ground-state orbitals in each of the anions $[VO(LL)_2]^{2-}$, where LL = edt, pdt, and $[VS(edt)_2]^{2-}$. The small reduction in the magnitude of the metal hyperfine parameters between **1** and **2** seems to be attributable mainly to vanadium 4s orbital admixture into the ground state of the latter. This is in contrast to the interpretation of the reduction of the hyperfine parameters in the compounds VE(salen) and VE(acen), where E = O, S, when the oxo group was replaced by the sulfido group.[10] These latter compounds were reported to give axially symmetric spin-Hamiltonian parameters. The changes in the hyperfine parameters were therefore attributed solely to a significantly smaller value of P in the sulfido compared to the oxo derivatives. This reduction in P implies a smaller formal charge on the vanadium atom in the sulfido derivative. In contrast to this our findings suggest that there is no significant change in the charge on the vanadium atoms in this series of vanadiuim thiolate anions $[VE(LL)_2]^{2-}$ (E = O, LL = edt, pdt; E = S, LL = edt).

The most notable change in the hyperfine parameters occurs when the terminal oxo group is replaced by the $OSiMe_3$ moiety. These changes are reflected in the compositions of the ground states. The increase in both the edt–sulfur character and P for **3** compared with **1** is consistent with the structural information and its interpretation, vide supra. The presence of the $OSiMe_3$ group also appears to cause a significant reduction in the symmetry of the anion, which leads to significant mixing between the vanadium d_{z^2}, 4s and $d_{x^2-y^2}$ orbitals.

A numerical analysis of the **g** tensors by the above minimization method was unsatisfactory due to the larger number of unknown parameters. Qualitatively, the small reduction in the mean value of g_{xx} and g_{yy} for **2** compared to **1** is almost proportional to changes in the energies of the peak maxima of the first band envelope in the electronic spectrum. This suggests that there are no major changes in the electronic structures of these two species. The most significant changes in the **g** tensor elements are those between **1** and **3**. The higher g_{zz} for **3** compared with **1** is qualitatively compatible with the putative increase in covalency in the basal VS_4 entity. Similarly the reduction in both g_{xx} and g_{yy} from **1** to **3** also correlate with the proposal that the $d_{x^2-y^2} \rightarrow d_{xz}, d_{yz}$ transition is lower in energy for **3** compared to **1**. Indeed the ratio of $1/\Delta E$ for this transition compared to the ratio of Δg_{ii}, where $i = x$ or y, for these two compounds are very similar. This indicates that the reduction in the $d_{x^2-y^2} \rightarrow d_{xz}, d_{yz}$ transition energy is the dominant contribution to g_{xx} and g_{yy} in these two complexes.

Spectrophotometric Monitoring of the Conversion of 1 to 2. Identification and spectroscopic characterization of complex **3** has allowed some insight into the mechanistic pathway for the conversion of **1** to **2** effected by $(Me_3Si)_2S$. Electronic spectral changes have proven a convenient means to follow the course of the reaction, for the three complexes have distinctly different spectral profiles. The spectral changes associated with reaction of **1** with 1 equiv of $(Me_3Si)_2S$ in DMF are shown in Figure 5. Injection of the silyl reagent into a cell containing a light green solution of **1** leads to *immediate* generation of an intense red-purple coloration. The absorption spectrum was recorded as soon as possible (ca. 30 s) after addition of silyl reagent and corresponded exactly in profile and intensity to that expected for complete conversion of **1** to **3**. This confirms the latter to be the first detectable product of the reaction and argues against addition of a Si—S bond across the V=O multiple bond to yield the six-coordinate species $[V(OSiMe_3)(SSiMe_3)(edt)_2]^{2-}$. The spectrum of **3** then slowly converts over 24 h to that of **2** but with no one single well-defined set of isosbestic points, indicating the intermediacy of additional species; it is indeed difficult to envisage how **3** could convert to **2** in a single, one-step process. On the basis of these spectral changes and the successful identification of **3**, we propose the mechanism of the reaction to be as shown in Scheme I. Nucleophilic attack by the vanadyl oxygen atom of **1** at electrophilic Si rapidly leads to formation of **3** and Me_3SiS^-. In subsequent slower steps, ligand exchange between **3** and Me_3SiS^- then leads to $[V(SSiMe_3)(edt)_2]^-$, followed by nucleophilic attack by liberated Me_3SiO^- at electrophilic Si to yield abstraction of Me_3Si^+ and formation of **2** and $(Me_3Si)_2O$. Two

(18) DeArmond, K.; Garret, B. B.; Gutowsky, H. S. *J. Chem. Phys.* **1965**, *42*, 1019.
(19) O'Reilly, D. E. *J. Chem. Phys.* **1958**, *29*, 1188.
(20) Golding, R. M. *Mol. Phys.* **1962**, *5*, 369.
(21) Atherton, N. M.; Winscom, C. J. *Inorg. Chem.* **1973**, *12*, 383.

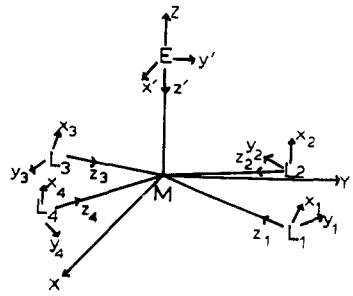

Figure 4. Axes system for $[ML_4]$. For each L_i the x_i axis is the ML_iE plane while on E x' and y' are parallel to the metal x and y axes, respectively.

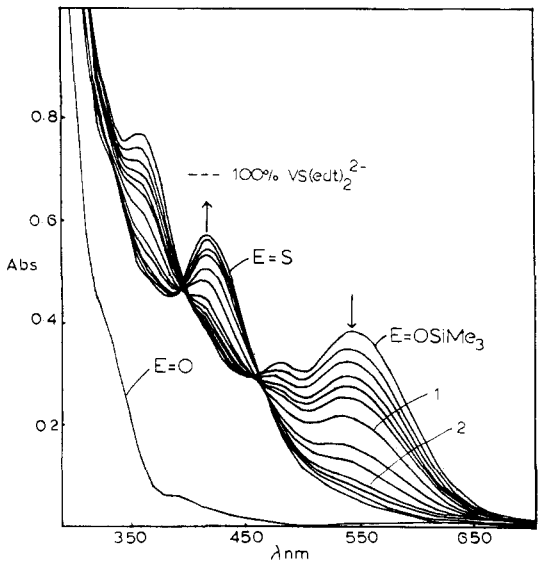

Figure 5. Electronic spectral changes for $[VE(edt)_2]^{-/2-}$ in DMF accompanying conversion of E = O (**1**) to E = $OSiMe_3$ (**3**) to E = S (**2**) by 1 equiv of $(Me_3Si)_2S$. The E = O trace contains no added silyl reagent. Recording of the initial E = $OSiMe_3$ trace was initiated ca. 30 s after silyl reagent addition. For clarity, only selected traces for the conversion of E = $OSiMe_3$ to E = S are shown; trace 1 was recorded after 2 h 45 min, trace 2 after 11 h 45 min, the limiting spectrum after 24 h 45 min. The theoretical absorption for complete conversion of E = O to E = S is shown as a dashed line.

Scheme I

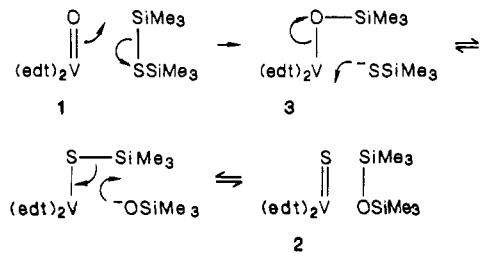

points warrant further comment: (i) Since **1** and $(Me_3Si)_2S$ are completely converted to **3** and Me_3SiS^-, further reaction to yield **2** must be between these two species and not somehow, for example, between Me_3SiS^- and **1**, for none of the latter remains. We were able to support this conclusion by reacting isolated **3** with 1 equiv of $NaSSiMe_3$; a slow reaction was observed that yielded orange-brown **2**, as confirmed by IR comparison of precipitated solid with authentic material. Addition of a second 1 equiv of $NaSSiMe_3$ does not affect the identity of the product. (ii) Reaction of **1** with 1 equiv of $(Me_3Si)_2S$ does not yield 100% conversion to **2**; the final absorbance of the 417-nm band in Figure 5 corresponds to only 74% of that expected for complete conversion to **2**. In order to determine if this behavior was due to an equilibrium, we treated a solution of **2** with 1 equiv of dried $(Me_3Si)_2O$ and observed a slow decrease in the absorbance at 417 nm, reaching a limiting value identical with that seen in Figure 5. The exact composition of the equilibrium mixture is difficult to determine given our current knowledge of the exact reaction mechanism and the paramagnetic nature of these species, ruling out NMR as an analytical probe. That **2** should react to a noticeable degree with $(Me_3Si)_2O$ further attests to the high reactivity of the $V{=}S^{2+}$ moiety.

Acknowledgment. This work was supported by NSF Grant CHE-8507748 (to G.C.). We thank the Bloomington Academic Computing Service for a gift of computer time. The diffractometer used for X-ray crystallography was funded by NSF Grant CHE-7709496. D.C., J.T., and F.E.M. thank the SERC for financial support.

Appendix

On the basis of the axis system in Figure 4 and C_{2v} point symmetry the antibonding molecular orbitals are

$$|a_1\rangle = \alpha_1(c_1 d_{x^2-y^2} + c_2 d_{z^2} + c_s 4s) - \alpha_1' \Pi_{a_1}(L) \quad \text{(A1)}$$

where

$$c_1^2 + c_2^2 + c_s^2 = 1 \qquad \alpha_1^2 + \alpha_1'^2 = 1 \quad \text{(A2)}$$

$$|a_2\rangle = \alpha_2 d_{xy} - \alpha_2' \sigma_{a_2}(L) \quad \text{(A3)}$$

$$|b_1\rangle = \beta_1 d_{xz} - \beta_1' p_x(E) - \beta_1'' \Pi_{b_1}(L) \quad \text{(A4)}$$

$$|b_2\rangle = \beta_2 d_{yz} - \beta_2' p_y(E) - \beta_2'' \Pi_{b_2}(L) \quad \text{(A5)}$$

$$|a'_1\rangle = \gamma(c_1 d_{z^2} - c_2 d_{x^2-y^2} + c_s' 4s) - \gamma' p_z(E) - \gamma'' \sigma_{a_1}'(L) \quad \text{(A6)}$$

$$\sigma_{a_2}(L) = c_\sigma(s_1 - s_2 + s_3 - s_4) + c_\sigma'(z_1 - z_2 + z_3 - z_4) \quad \text{(A7)}$$

$$\Pi_{a_1}(L) = c_n(s_1 + s_2 + s_3 + s_4) + c_n'(-y_1 + y_2 - y_3 + y_4) \quad \text{(A8)}$$

$$\Pi_{b_1}(L) = c_{\Pi_1}(s_1 - s_2 - s_3 + s_4) + c_{\Pi_1}'(x_1 - x_2 - x_3 + x_4) \quad \text{(A9)}$$

$$\Pi_{b_2}(L) = c_{\Pi_2}(s_1 + s_2 - s_3 - s_4) + c_{\Pi_2}'(x_1 + x_2 - x_3 - x_4) \quad \text{(A10)}$$

where s_i, x_i, y_i, and z_i represent the s and p orbitals on the ith ligand atom.

The **g** and **A** tensor elements are derived by considering spin–orbit coupling, the electronic Zeeman effect and metal hyperfine coupling as consecutive perturbations. In the spin–orbit coupling calculation the effects of spin–orbit coupling on the ligand atoms L and on the metal have been considered, but not that in the overlap region. Also when transforming angular momentum operators from the metal to ligand centers we have neglected terms involving the metal to ligand translation and overlap contributions.

With $|a_1\rangle$ as the ground state, using the equations

$$g_{zz} = 2\langle \bar{A}_1 | \hat{l}_z + 2.0023 \hat{s}_z | A_1 \rangle$$

$$g_{xx} = 2\langle \bar{A}_1 | \hat{l}_x + 2.0023 \hat{s}_x | \bar{A}_1 \rangle$$

$$g_{yy} = 2i\langle \bar{A}_1 | \hat{l}_y + 2.0023 \hat{s}_y | \bar{A}_1 \rangle$$

$$A_{zz} = 2P\langle \bar{A}_1 | \hat{l}_z - \kappa \hat{s}_z + \tfrac{1}{7}\hat{a}_z | A_1 \rangle$$

$$A_{xx} = 2P\langle \bar{A}_1 | \hat{l}_x - \kappa \hat{s}_x + \tfrac{1}{7}\hat{a}_x | \bar{A}_1 \rangle$$

$$A_{yy} = 2Pi\langle \bar{A}_1 | \hat{l}_y - \kappa \hat{s}_y + \tfrac{1}{7}\hat{a}_y | \bar{A}_1 \rangle$$

where $\hat{a}_j = 4\hat{s}_j - (\hat{l}\cdot\hat{s})\hat{l}_j - \hat{l}_j(\hat{l}\cdot\hat{s})$, where $j = x, y$, or z and $|\overset{+}{\bar{A}}_1\rangle$ is the ground state modified by spin–orbit mixing, we have

$$g_{zz} = 2.0023 - \frac{8\alpha_2\alpha_1 c_1}{\Delta a_2} \times [\alpha_2\alpha_1 c_1\zeta_m - 2\alpha_2'\alpha_1' c_n' c_\sigma'\zeta_L(\cos(\theta - 90))] \quad \text{(A11)}$$

$$g_{xx} = 2.0023 - \frac{2}{\Delta b_2}[\alpha_1\beta_2\zeta_m(c_1 + 3^{1/2}c_2) + 4\beta_2''\alpha_1' c_{\Pi_2}' c_n'\zeta_L(\cos(\theta - 90))(\cos\phi)][\alpha_1\beta_2(c_1 + 3^{1/2}c_2) + 4\beta_2''\alpha_1' c_{\Pi_2}' c_n'(\cos(\theta - 90))(\cos\phi)] \quad \text{(A12)}$$

$$g_{yy} = 2.0023 - \frac{2}{\Delta b_1}[\alpha_1\beta_1\zeta_m(c_1 - 3^{1/2}c_2) + 4\beta_1''\alpha_1' c_{\Pi_1}' c_n'\zeta_L(\cos(\theta - 90))(\sin\phi)][\alpha_1\beta_1(c_1 - 3^{1/2}c_2) + 4\beta_1''\alpha_1' c_{\Pi_1}' c_n'(\cos(\theta - 90))(\sin\phi)] \quad \text{(A13)}$$

$$A_{zz} = \bar{A} + P\left[\frac{2}{3}\Delta g_{zz} - \frac{1}{3}(\Delta g_{xx} + \Delta g_{yy}) - \frac{4\alpha_1^2}{7}(c_1^2 - c_2^2) + \frac{3c_1 + 3^{1/2}c_2}{14(c_1 - 3^{1/2}c_2)}\Delta g_{yy} + \frac{3c_1 - 3^{1/2}c_2}{14(c_1 + 3^{1/2}c_2)}\Delta g_{xx}\right] \quad \text{(A14)}$$

$$A_{xx} = \bar{A} + P\left[\frac{2}{3}\Delta g_{xx} - \frac{1}{3}(\Delta g_{yy} + \Delta g_{zz}) + \frac{2\alpha_1^2}{7}(c_1^2 - c_2^2 - 2(3^{1/2})c_1c_2) + \frac{3^{1/2}c_2}{14c_1}\Delta g_{zz} - \frac{3c_1 + 3^{1/2}c_2}{14(c_1 - 3^{1/2}c_2)}\Delta g_{yy}\right] \quad \text{(A15)}$$

$$A_{yy} = \bar{A} + P\left[\frac{2}{3}\Delta g_{yy} - \frac{1}{3}(\Delta g_{xx} + \Delta g_{zz}) + \frac{2\alpha_1^2}{7}(c_1^2 - c_2^2 + 2(3^{1/2})c_1c_2) - \frac{3^{1/2}c_2}{14c_1}\Delta g_{zz} - \frac{3c_1 - 3^{1/2}c_2}{14(c_1 + 3^{1/2}c_2)}\Delta g_{xx}\right] \quad \text{(A16)}$$

$$\bar{A} = P\left[-\kappa + \frac{1}{3}(\Delta g_{zz} + \Delta g_{xx} + \Delta g_{yy})\right] + A_{4s}\alpha_1^2 c_s^2 \quad \text{(A17)}$$

$$\Delta g_{ii} = g_{ii} - 2.0023$$

$P = gg_N\beta_N\beta\langle r^{-3}\rangle$ where r is the radial extension of the 3d orbitals. A_{4s} = the hyperfine splitting constant for an electron in the metal 4s orbital. κ = isotropic Fermi contact contribution.

Registry No. $(PPh_4)Na(1)$, 97689-50-4; $(PPh_4)Na(2)$, 97689-52-6; $(PPh_4)(3)$, 104834-06-2; $NaSSiMe_3$, 87495-22-5; $Na_4(acac)_2[VO(pdt)_2]$, 104834-08-4; $VO(acac)_2$, 3153-26-2; $(NMe_4)Na[VO(pdt)_2]$, 104834-09-5; $(Me_4N)Na[VO(edt)_2]$, 89061-83-6; $(PPh_4)Na[VO(pdt)_2]$, 104834-10-8; hexamethyldisilathiane, 3385-94-2.

Supplementary Material Available: Complete listings of atomic coordinates, isotropic and anisotropic thermal parameters, and interatomic distances and angles (8 pages); listings of calculated and observed structure factors (10 pages). Ordering information is given on any current masthead page. A complete crystallographic structure report (MSC Report 84105) is available on request from the Indiana University Chemistry Library.

Contribution from the Chemistry Department, Columbia University, New York, New York 10027, and Istituto di Strutturistica Chimica, Centro di Studio per la Strutturistica Diffrattometrica del CNR, Università di Parma, 43100 Parma, Italy

How a Bifunctional Complex Drives Reactivity of CO_2-like Molecules: Sodium [*N*,*N*′-Ethylenebis(salicylaldiminato)]cobaltate(I) Promotion of the Reductive Coupling of Molecules Resembling CO_2

Francesco Arena,† Carlo Floriani,*† A. Chiesi-Villa,‡ and Carlo Guastini‡

Received March 17, 1986

The bifunctional complex [Co(salen)Na(THF)] (**1**, salen = *N*,*N*′-ethylenebis(salicylaldiminato) dianion) promotes the reductive coupling of methyl pyruvate, diethyl ketomalonate, and *p*-tolylcarbodiimide via a C–C bond formation. Methyl pyruvate is transformed in diastereomeric dimethyl dimethyltartrates and *p*-tolylcarbodiimide into tetra-*p*-tolyloxalamidine, while **1** is oxidized to [Co(salen)]. A free-radical pathway involving the homolytic cleavage of a Co–Co σ bond is suggested. Reaction of **1** with diphenylketene, DPK, suggests an alternative pathway for the reductive coupling of CO_2-like molecules. The reaction occurs in a 1:1 DPK/Co molar ratio and gives $\{[Co(salen)]_2Na_2[Co(salen(DPK)_2)]\}\cdot 3THF$ (**8**), which is a trinuclear cobalt(II) complex containing two intact [Co(salen)] units bridged by two Na^+ ions to a third cobalt(II) unit, where the metal is surrounded by a hexadentate ligand resulting from the addition of two DPK molecules to the same imino group of the salen ligand. The X-ray analysis shows a rather close proximity between the carbon atoms belonging to the two DPK molecules as in a precoupling stage. Any C–C bond formation between those carbon atoms will restore the original imino functionality in the salen ligand. This may be another plausible pathway leading to a C–C bond between CO_2-like molecules. Processes involving reactive sites and electron transfers from an aromatic polydentate ligand surrounding a metal are very important in compounds driving reactions of small molecules. Complex **1** promotes the usual reductive disproportionation of aryl isocyanates, RNCO (R = phenyl, 1-naphthyl). Crystallographic details for complex **8**: space group $P\bar{1}$ (triclinic); $a = 16.313$ (2) Å; $b = 19.164$ (3) Å; $c = 15.020$ Å; $\alpha = 107.16$ (2)°; $\beta = 113.23$ (2)°; $\gamma = 102.06$ (2)°; $Z = 2$; $D_{calcd} = 1.410$ g cm^{-3}. The final R factor was 0.085 for 2742 observed reflections.

Introduction

General objectives in the activation of carbon dioxide by transition-metal complexes are the formation of M–C and C–C bonds. The latter bond can be achieved either by a reductive coupling or by the incorporation of CO_2 into an organic substrate.[1-4] It must be pointed out, however, that the majority of

† Columbia University.
‡ Univesità di Parma.

(1) Sneeden, R. P. A. In *Comprehensive Organometallic Chemistry*; Wilkinson, G., Stone, F. G. A., Abel, E. W., Eds.; Pergamon: Oxford, 1982; Vol. 8, Chapter 50.4, pp 225–283.

0020-1669/86/1325-4589$01.50/0